Journal of Hydrology: Regional Studies 41 (2022) 101106

Contents lists available at ScienceDirect

Journal of Hydrology: Regional Studies

journal homepage: www.elsevier.com/locate/ejrh

Spatio-temporal dynamics of suspended particulate matter in the middle Niger River using in-situ and satellite radiometric measurements

Moussa Boubacar Moussa [a,b,*], Amadou Abdourhamane Touré [a], Laurent Kergoat [b], Bruno Lartiges [b], Emma Rochelle-Newall [c], Elodie Robert [d], Marielle Gosset [b], Bachir Alkali Tanimoun [e], Manuela Grippa [b]

[a] Abdou Moumouni University, Faculty of Science and Technology (FAST) - Department of Geology, PB 10662 Niamey, Niger
[b] Géosciences Environnement Toulouse (GET, UMR 5563 / Paul Sabatier University Toulouse III / CNRS / IRD / CNES), France
[c] Sorbonne Université, Univ Paris Est Creteil, IRD, CNRS, INRAé, Institute of Ecology and Environmental Sciences of Paris (iEES-Paris), 4 Place Jussieu, 75005 Paris, France
[d] LETG-Nantes (UMR 6554 CNRS, Université de Nantes, France
[e] Niger Basin Authority (NBA), Niamey, Niger

ARTICLE INFO

Keywords:
Middle Niger River
Suspended particulate matter
Optical remote sensing
Discharge
Kaolinite
Sentinel-2 MSI data

ABSTRACT

Study Region: Middle Niger River Basin (MNRB), Ansongo to Niamey, Sahel, West Africa.

Study Focus: Although MNRB hydrology and the red flood phenomena have been addressed in the past literature, water quality parameters and suspended particulate matter (SPM) dynamics remain poorly known. SPM impacts dam silting, exacerbating flooding, and microbial water quality. This study couples in-situ SPM measurements to radiometric measurements by in-situ and satellite sensors to analyse the temporal and spatial evolution of SPM in the MNRB and assess the contribution of the local flood (red flood) to SPM in Niamey.

New Hydrological Insights for the Region: SPM is composed of very fine kaolinites with a major mode around 200–300 nanometers which results in high reflectance in the visible and infrared bands. Radiometric measurements by both radiometer and Sentinel-2 MSI sensors are well correlated to in-situ SPM, allowing efficient spatio-temporal monitoring of SPM concentration. SPM increases very rapidly at the beginning of the rainy season, reaching a peak, characterized by very high SPM values, about one month before the red flood. Satellite data highlight the significant contribution of the right bank tributaries to SPM in the MNRB during this period. SPM then decreases and remains low despite the second runoff increase (black flood) arriving in Niamey after the end of the rainy season from the upper basin.

1. Introduction

The Niger River basin plays a major cultural, historical and socio-economical role in West Africa (Autorité du Bassin du Fleuve Niger ABFN, 2018). It is home to more than 130 million people throughout nine countries (Niger Basin Nexus profile, 2018). The river

* Corresponding author at: Abdou Moumouni University, Faculty of Science and Technology (FAST) - Department of Geology, PB 10662 Niamey, Niger.
E-mail addresses: mboubacar63@gmail.com, moussa.boubacar@get.omp.eu (M. Boubacar Moussa).

https://doi.org/10.1016/j.ejrh.2022.101106
Received 18 January 2022; Received in revised form 8 May 2022; Accepted 9 May 2022
Available online 20 May 2022

is an essential resource for drinking water, fishing, irrigation, hydroelectric power generation, and navigation/transportation (Dieye et al., 2020; Droy and Morand, 2013; Paturel et al., 2020). Moreover, many large cities are located on the banks of the Niger River, such as Bamako (2.71 million people in 2020) in Mali and Niamey (1.3 million people in 2020) in Niger (worldpopulationreview, 2022).

The Niger River originates in the humid Guinean zone, which receives more than 2000 mm of rain per year and the basin is divided into four units (Fig. 1): the upper Niger, the inner delta, the middle Niger and the lower Niger (Amogu, 2009). In its middle part, the river runs more than 1000 km through the Sahelian region and shows distinct flow regime at different locations. At Ansongo, located in Mali about 350 km upstream of Niamey, the annual hydrograph displays one discharge peak typically occurring between October and March (Olivry, 2002). This flood (black flood) has its origins in water contributions from the upper basin and arrives at Ansongo well after the end of the rainy season because of a two-to-three months residence time in the inner Niger delta. Two different discharge peaks are observed in Niamey (Fig. 2). In addition to the previous flood, a large second flood (the red flood) occurs during the local rainy season typically between June and September (Amani and Nguetora, 2002). This flood is the result of rainfall and water inputs from tributaries located downstream of Ansongo in the middle part of the Niger River basin. The low water period in Niamey extends between April and May.

The Sahelian part of the Niger River watershed is very sensitive to climatic variations and anthropogenic constraints (Nicholson et al., 1998). Since the 1960's, this region has experienced rainfall deficits (beginning in the late 1960's to 1990's) of 20–40% and a retreat of isohyets (1970–1989) over 200 km to the south (Hulme et al., 2001; Lebel and Ali, 2009). Severe droughts in the early 1970's and the early mid 1980's led to a decrease in vegetation cover and an increase of erosion processes (Descroix et al., 2012; Descroix et al., 2015; Descroix et al., 2018; Janicot et al., 1996). In 1985, the Niger River even stopped flowing in Niamey (Billon, 1985). After the drought period, the vegetation globally recovered following the return of precipitations (Dardel et al., 2014a, Dardel et al., 2014b). However, some small areas show a persistent decrease in vegetation cover and, consequently, an increase in surface runoff (Descroix et al., 2018; Gal et al., 2017).

In addition, the MNRB is a highly populated area. Strong demographic growth (3.8% per year in Niger over the last seven decades, World Bank, 2017) has led to an extension of cultived areas and an intensification of natural resource exploitation (forest, savannah, rangeland) (Leblanc et al., 2008; Tidjani, 2008). The deforestation in these areas has increased the amount of bare surfaces and weakened the Sahelian soils that undergo erosive actions of wind and rain (Abdourhamane Touré et al., 2010). Overall, changes in land cover, due to climatic variations and/or anthropogenic factors, have led to a general increase in runoff and have caused endorheism breaks in the middle Niger River watershed (Amogu et al., 2010; Descroix et al., 2018; Favreau et al., 2009; Mahé et al., 2013). An example of this situation is the intensification of the red flood phenomenon that was observed in Niamey after the 90's and the recurrent floodings occurring in Niamey, causing severe damage in the river plain (Cassé et al., 2016; Mahamadou et al., 2018). The greatest flood ever registered in Niamey was recorded in 2020 (Lebel et al., 2020; Tiepolo et al., 2021, Fig. 2).

Past, ongoing and future changes in the Niger River hydrology are supposed to deeply affect water resources but also water quality parameters. In particular, increased erosion and/or increase in precipitation amount and intensity (Panthou et al., 2018; Taylor et al., 2017) would lead to an increase of sediment transport and of suspended particulate matter (SPM) in surface waters. This would impact

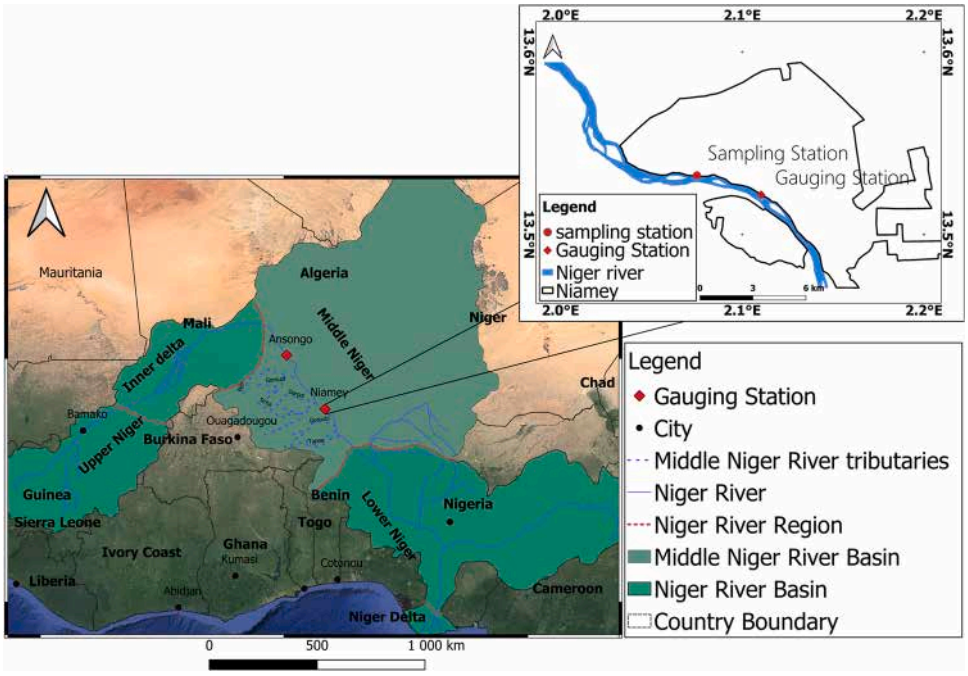

Fig. 1. Study area with the location of the in-situ SPM, radiometric measurement sampling points and.
showing input from the Sirba tributary.

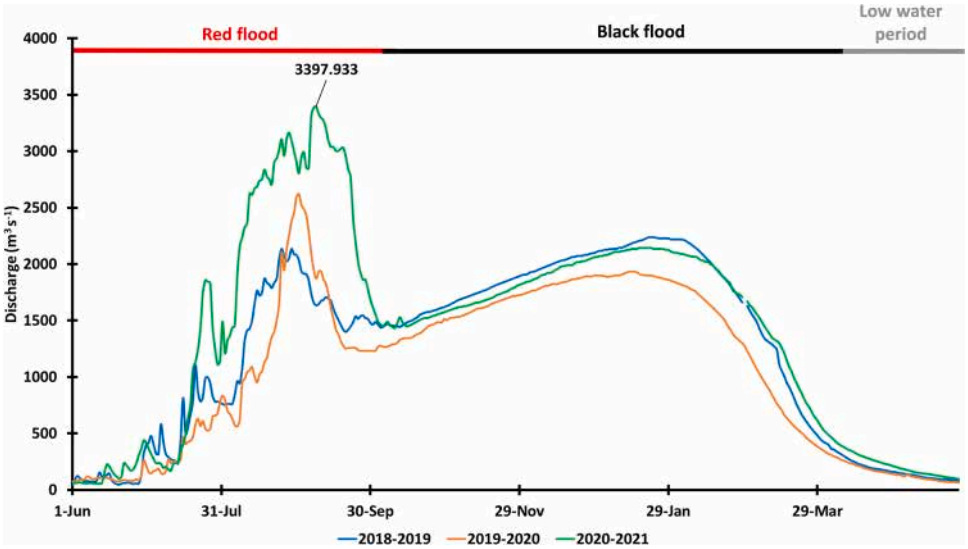

Fig. 2. Niger River hydrographs at the Niamey hydrological station (2018–2021).

in turn water flow and dam silting with further consequences on floods. In addition, SPM plays also an important role on aquatic ecosystems (i.e. Hauer et al., 2018; Pennock and Sharp, 1994) and human health by facilitating the transport and the development of pathogens (Robert et al., 2021; Rochelle-Newall et al., 2015; Zheng and DiGiacomo, 2017).

If the Niger River hydrology and the red flood phenomena have been widely addressed in the literature from a quantitative point of view, water quality and SPM monitoring has received much less attention. Measurements of SPM in the Niger River basin are generally sparse and limited in time. In the middle part of the Niger watershed, the earliest SPM measurements were carried out between 1976 and 1982 for the feasibility study of a dam at Kandadji (Gallaire, 1995). More recently, Amogu (2009) reported SPM concentrations in the middle Niger and Alhou et al. (2016) recorded two years (fortnightly sampling from April 2011 to March 2013) of SPM measurements at Niamey. However, a detailed assessment of the spatio-temporal dynamics of SPM at a fine temporal scale has yet to be done. This study fills this information gap by providing SPM at a daily scale and during several hydrological cycles.

Remote sensing techniques have been developed for inland water studies in the last 20 years to provide estimates of SPM variability in space and time. Data from optical radiometers detect near-surface sediments, but this information has been successfully used to assess total suspended solid and sediment transport in various rivers (Martinez et al., 2009; Nechad et al., 2010; Petus et al., 2010; Pinet et al., 2017). Most of the studies addressing SPM dynamics in rivers use data from medium resolution sensors such as the MEdium Resolution Imaging Spectrometer (MERIS) and Moderate Resolution Imaging Spectroradiometer (MODIS) because a high temporal frequency is necessary to correctly sample the rapid dynamics of rivers. However, their coarse spatial resolution [ranging from 250 m in the visible and the Near-infrared (NIR) to 1 km in the Short Wave InfraRed (SWIR) bands for MODIS is not sufficient to accurately monitor the Niger River, particularly during low water periods when river reaches are narrower. Only recently have high resolution satellite data been available at the temporal frequency necessary to monitor SPM over smaller dynamics rivers. In particular, the MultiSpectral Instrument (MSI) sensor on-board the Sentinel-2 provides data every 5 days at a 10 m spatial resolution in the visible and near infrared bands and 20 m in the SWIR bands. Such data have proved efficient to monitor SPM dynamics in different water bodies (i.e. Caballero et al., 2018; Liu et al., 2017; Pahlevan et al., 2017). Several algorithms have been developed to retrieve SPM from radiometric measurements from satellite over turbid waters using theoretical (Nechad et al., 2010) semi-empirical (Shen et al., 2010) and empirical approaches, mostly site specifics (Doxaran et al., 2002; Robert et al., 2017; Caballero et al., 2018; Li et al., 2019; Renosh et al., 2020). Employing wavelengths in the NIR domain, in combination with those in the visible range (Li et al., 2019) or alone (Robert et al., 2017), has been shown useful to avoid saturation for high SPM values. Switching algorithms (Shen et al., 2010; Han et al., 2016; Novoa et al., 2017; Caballero et al., 2018; Renosh et al., 2020) have been proved efficient to address a wide range of SPM values.

Until now, few studies have focused on the Sahelian region as it is quite challenging for optical remote sensing. This is because on the one hand, the very high atmospheric aerosol loading (mineral dust and biomass burning) and the highly variable water vapor content make atmospheric corrections difficult and, on the other hand, the very high values of reflectance of West African waters challenge inversion algorithms classically used in other regions. Some encouraging result have been obtained on a few lakes using data from LANDSAT (Kaba et al., 2014; Robert et al., 2016; Robert et al., 2017) and Sentinel-2 MSI (Robert et al., 2021) but further validation, especially for rivers, is needed.

The main objective of this work was to analyse the spatio-temporal dynamics of SPM in the middle Niger River together with the hydrological variability and water discharge at Niamey and in the upstream part of the basin. To do this, we first assess the potential of radiometric measurements by both an in-situ SKYE radiometer and Sentinel-2 MSI to monitor SPM in this area. SKYE data are then employed to complete the temporal series of SPM sampled in-situ to get daily time series over three years. Finally, Sentinel-2 MSI data

are used to explore the spatial variability of SPM in the middle Niger River and to assess the overall contribution of the red flood to SPM arriving at Niamey.

2. Material and methods

2.1. Study site

In-situ measurements were carried out in Niamey located downstream of the confluences of some major middle Niger River tributaries like the Sirba, the Dargol and the Gorouol (Fig. 1). The area is characterized by a semi-arid tropical climate with well-marked contrasting seasons: a rainy season (May - September) and a dry season (October - April). The average rainfall between 1970 and 2017 in Niamey was equal to 527,36 mm per year (Hamadou Younoussa et al., 2020). The Potential Evapotranspiration (ETP) is around 3000 mm per year (Allies et al., 2020). In Niamey, two drinking water treatment plants ensure the supply of the potable water, 72% of which is provided by the Goudel station (our sampling site) with remaining water provided by the Yantala station. Both plants are located on the left bank of the Niger River.

Discharge data were obtained from the Niger Basin Authority (NBA). The flow rate is measured daily at 00:00 with an automatic hydrometer SEBA PS Light 2GSM. The data used in this study cover three hydrological cycles between 2018 and 2021 (Fig. 2). During this period, maximum discharge was 2136 $m^3 s^{-1}$, 2620 $m^3 s^{-1}$ and 3998 $m^3 s^{-1}$ for the red floods of 2018, 2019 and 2020, respectively. The record value in 2020 is the highest discharge peak ever measured since the station was built in 1929, largely exceeding the previous 2492 $m^3 s^{-1}$ record of 2012 (Lebel et al., 2020). The maximum discharge recorded for the black flood during this study was the 22th of January 2019 with 2238 $m^3 s^{-1}$. The low water period occurring between April and May with very low discharges (60 $m^3 s^{-1}$ in April 2020).

2.2. Suspended particulate matter (SPM) measurements

SPM measurements were conducted between July 17, 2018 and August 16, 2020. River water samples were collected between 10 a.m. and 1 p.m. from the top 20 cm of the water column in 500 mL bottles. The sampling point (lat 13.520313 North, lon 2.066145 East) is located on the left bank and is approximately 7 m from the shoreline (Fig. 1). The river water was collected at different time steps to follow the hydrological variability. During the red flood, the sampling time step was daily from July 1 to August 15, 2019 and every 2nd day from July 1 to August 15, 2020. Outside the red flood period, the sampling time step varied from one week until the end of the rainy season to one month during the remaining of the hydrological cycle.

The sampled water was homogenized and then 50 mL were collected and filtered through a Whatman fiberglass filter with a porosity of 0.7 μm. The filters were previously heated to 105 °C and weighed. The sediment deposited on the filter was heated again at 105 °C for 1h30 and then re-weighed.

The SPM concentration was calculated for each sampling date from the SPM mass and the volume of filtered water Eq. (1).

$$[SPM] = (Mfs - Mf) / Vw \quad (1)$$

where Mfs is the Filter mass with sediment; Mf is the Original filter mass; Vw is the filtered water volume.

Two or three replicates were made for each water sample and averaged to reduce noise and check consistency.

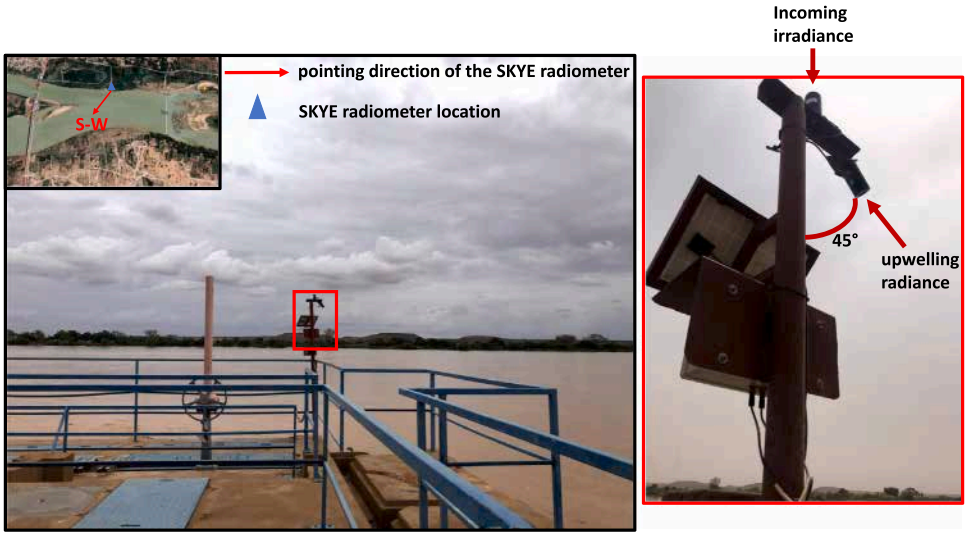

Fig. 3. SKYE radiometer at the Sampling station monitoring Niger River water reflectance.

The particle size distribution and mineralogy of sediments were assessed over few water samples collected during the black flood (2017–10–06 and 2017–10–24) and the red flood (2018–07–03, 2018–07–08, 2018–07–09 and 2019–08–06). The particle size distribution was measured with a Partica LA-950V2 laser granulometer (Partica LA950-V2, Horiba, 2022). The particles were also observed with a JEOL JEM 2100 F Transmission Electron Microscope (TEM) with an operating voltage of 200 kV and a resolution of 2.3 Å (CMOS Gatan RIO 16IS 4 K camera). The mineralogy was determined using EDXS Analysis (Ultim Max TEM 80 mm^2 Windowless – Oxford Instruments). For TEM imaging and microanalysis, the sample was resuspended under ultrasonication, a drop of suspension was deposited on a formvar-coated copper grid, and excess water was blotted with filter paper.

2.3. Niger River water reflectance

The Niger River water reflectance was measured in situ with a SKYE radiometer installed at the water sampling point location since July 2018. The radiometer is composed of two sensors (SKR1840D/I Two channel Sensor, SKYE Instruments Ltd, Wales, UK) measuring the incoming radiation in the red and infrared bands at the same wavelengths as the Sentinel-2 MSI sensor, centred at 665.4 nm and 829.0 nm. Data were recorded every 30 min with a datahog2 + (SKYE). One sensor steered to the southwest looks at the water surface at a 45° angle (Fig. 3) to measure the total radiance (IFOV 25°, sensor height 2 m above the highest water), the other one measures the incoming irradiance (cosine response sensor to integrate hemispherical irradiance). Remote sensing reflectance is computed as the ratio of up-welling radiance by incoming irradiance and then multiplied by a factor π to give the dimensionless surface reflectance Eq. (2) to be compared to Sentinel-2 MSI surface reflectance. Total up-welling radiance comprises water-leaving radiance and specular reflection at the water surface caused by skyglint.

$$\rho = \pi * Rrs = \pi * L / Ed \quad (2)$$

where ρ is the SKYE radiometer surface reflectance (dimensionless), Rrs the SKYE remote sensing reflectance (sr^{-1}), L is the total observed radiance (μmol sr^{-1} m^{-2} s^{-1}) and Ed the down-welling irradiance (μmol m^{-2} s^{-1}).

Sentinel-2 MSI data are collected by two polar orbiting satellites (Sentinel-2A and Sentinel-2B launched in 2015 and 2017, respectively) placed on the same orbit, allowing a revisit time of 5 days at the equator. They carry a multi spectral instrument (Drusch et al., 2012) with four bands at 10 m, six bands at 20 m, and three bands at 60 m spatial resolution. For this work we used the three visible bands (bands 2, 3, and 4 respectively at 490 nm, 560 nm and 665 nm), and the near infrared band (NIR, band 8 at 842 nm) at 10 m spatial resolution, as well as the shortwave infrared band (band 12 at 2190 nm) at 20 m spatial resolution.

Sentinel-2 MSI surface reflectance (level 2 A) products are made available over the study area by the THEIA land data center (**www.theia-land.fr**). They are corrected for atmospheric effects using the MACCS-ATCOR Joint Algorithm (MAJA) processing chain (Hagolle et al., 2015). The processing chain (Hagolle et al., 2017) analyses temporal series of Level-1 C images and ancillary data to detect clouds and clouds shadows, to estimate the atmospheric optical thickness (including aerosols), the adjacency effects (including atmospheric scattering and multiple reflections between the surface and the atmosphere), and to apply a terrain correction based on topography. The atmospheric corrections are performed for pixels classified as land and extrapolated for pixels classified as water. The MAJA processing chain has been developed for land surface reflectance. It benefits from previous algorithm evaluations and is widely used. Other atmospheric corrections schemes exist, some targeting aquatic surface specifically (Kuhn et al., 2019; Pahlevan et al., 2021).

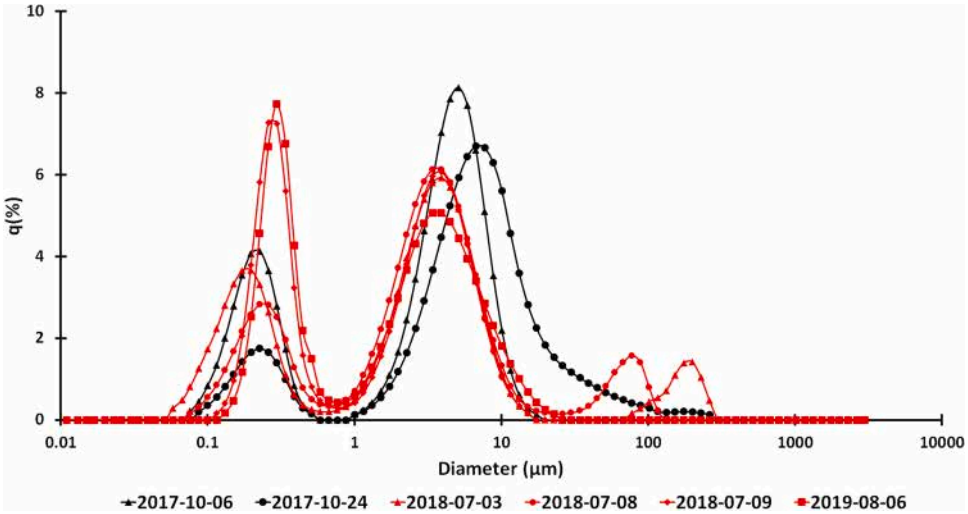

Fig. 4. Volumetric distribution of suspended particulate matter samples collected during the red flood (2018–07–03, 2018–07–08, 2018–07–09 and 2019–08–06) and the black flood (2017–10–06 and 2017–10–24) with SPM concentration equal to respectively 2.34 g L^{-1}, 1.44 g L^{-1}, 0.71 g L^{-1}, 1.034 g L^{-1}, 0.065 g L^{-1} and 0.073 g L^{-1}.

SPM is only retrieved for clear-sky pixels classified as open water. Sentinel-2 MSI pixels not already masked by the MAJA chain as clouds, aerosols or cloud shadows are classified as water pixels if the Modified Normalized Difference Water Index (MNDWI which is calculated as the difference between the green band and the SWIR band divided by their sum) is lower than 0.2 (Robert et al., 2017). An additional threshold on the green band reflectance is added to avoid unmasked residuals clouds (values lower than 0.4 are retained).

In order to avoid possible land-adjacency effects the Sentinel-2 MSI data employed at the Goudel sampling station and at the Ansongo site were averaged over a square box three pixels away from the shores.

Measurements of SPM concentration made at a day difference (day before and day after) with the satellite acquisition were considered in order to increase the number of match-ups (10 dates).

3. Results

3.1. SPM nature and granulometric sizes

Over the study period SPM concentration ranges from 0.01 g L^{-1} to 1.9 g L^{-1}. The lowest concentrations occur at the beginning of the dry season (mean = 0.0416 g L^{-1} and standard deviation = 0.0324 g L^{-1} calculated over the 1st October – 28th February 2019 period). The SPM concentration slightly increases over the March-May period and then more rapidly at the onset of the red flood, from June onwards, to reach its maximum, around 2 g L^{-1}, in July.

The term "Suspended Particulate Matter" is used here for particles suspended in a water column from the nano-scale to sand-sized sediments (Bilotta et al., 2012). Niger River SPM's size distributions curves reveal two well-pronounced modes during the red flood (Fig. 4). The two modes are centred around 0.172–0.296 and 3.9 μm ranging from medium sands to ultrafine clay particles. During the black flood, the same modes were found with less fine particles now centred around 0.26 μm and the larger one around 5.12–6.72 μm. These fine particles are often associated in aggregates (Fig. 5) and are predominantly composed of kaolinite, and iron oxyhydroxides,

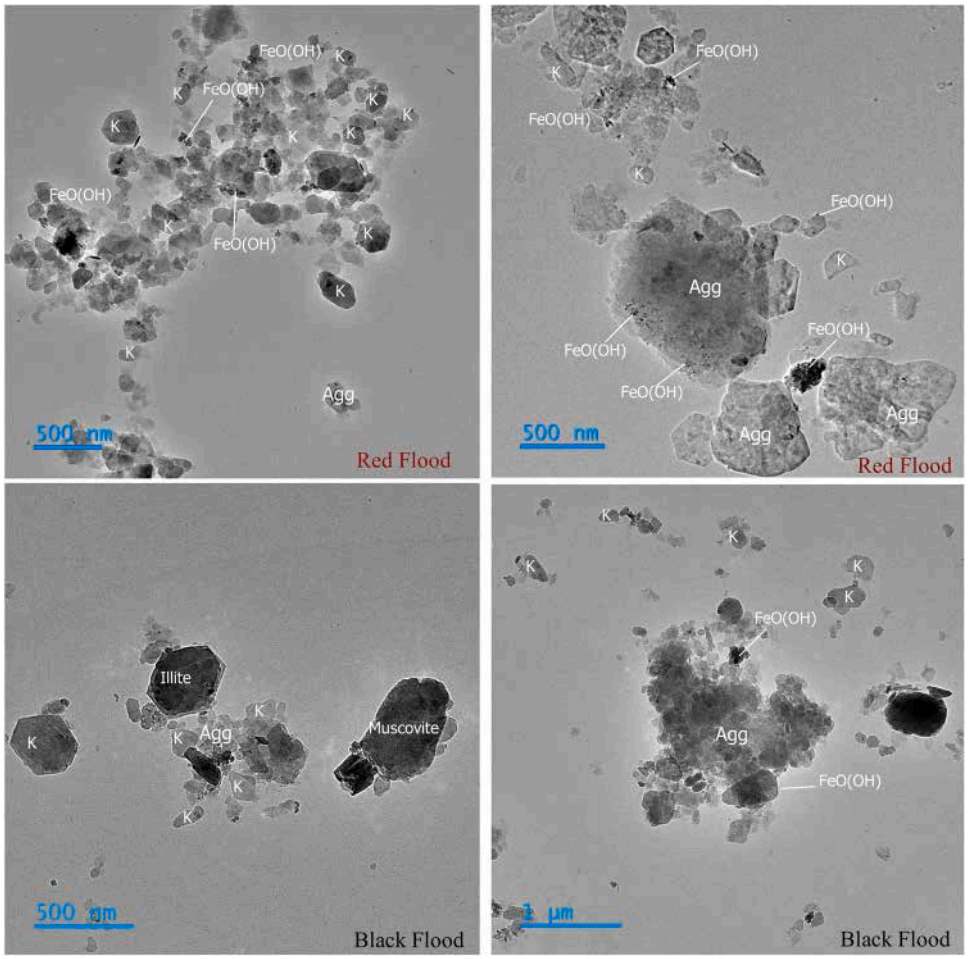

Fig. 5. Suspended Particulate Matter images obtained by the transmission electron microscope (TEM): red and black flood water samples. K: Kaolinite; Agg: Aggregate; FeO(OH): Iron Oxyhydroxide.

with minor occurrences of quartz, illite/muscovite, and ilmenite. Trace amounts of organic matter were also observed in the red flood samples.

3.2. Monitoring SPM with in-situ and satellite radiometry

Within a day, the temporal evolution of the SKYE radiometer reflectance is relatively constant in the morning but presents important peaks in the afternoon, more or less pronounced according to the period of the year, due to sunglint effect (i.e. specular reflection of direct sun radiation) observed on the red and NIR bands. This is consistent with the SKYE acquisition geometry and the sensor looking toward the south-west (Fig. 3). Sunglint effects are also observed on the band ratio NIR/red (Fig. 6). For each day, reflectance data were therefore averaged over the 9–11 a.m. period only, which corresponds to the time range with constant data, and sun-target-sensor geometry less prone to glint effect (glint angle larger than 50° at 10 h, relative azimuth in the 80°−160° interval). In addition, the match-up interval between morning radiometer data and SPM collection times is of the order of 2 h. Considering 9–11 h averages does not eliminate skyglint.

SKYE radiometer daily reflectance is then compared to Sentinel-2 MSI reflectance. Satellite and in situ data are well correlated in both the red and the NIR band (Fig. 7). The coefficient of determination r^2 is 0.93 and 0.92, for the red and the NIR, respectively, the RMSD (root mean square difference) 0.02 and 0.03 and MAPE (Mean Absolute Percentage Error) 9.3% and 63.8%.

Reflectance measured by both the SKYE and the Sentinel-2 MSI sensors in the red and NIR bands showed a strong seasonality with extremely high values (Fig. 8), reaching 0.35–0.40 during the rainy season (June-September), that are rarely encountered in large rivers. The yearly maxima for the three years of the study period were similar. MSI value are generally higher than SKYE values during the dry season at the end of March beginning of April particularly on the NIR band, as is also apparent by the scatter in low NIR values shown in Fig. 7. This is likely due to the impact of high aerosol content, which is quite important at this period due to Harmattan wind coming from the Sahara desert and is probably not completely corrected by the MAJA scheme.

SPM concentrations measured in situ are strongly correlated with reflectance or reflectance ratio.

The best fit is obtained using power relationships between SPM and the NIR band for Sentinel-2 MSI (RMSE = 0.19; MAPE = 36.7%; n = 25) and SPM and the NIR/red index for the SKYE radiometer (RMSE = 0.17; MAPE = 30.6%; n = 125) [Fig. 9a, b, Eqs. (3) and (4) below].

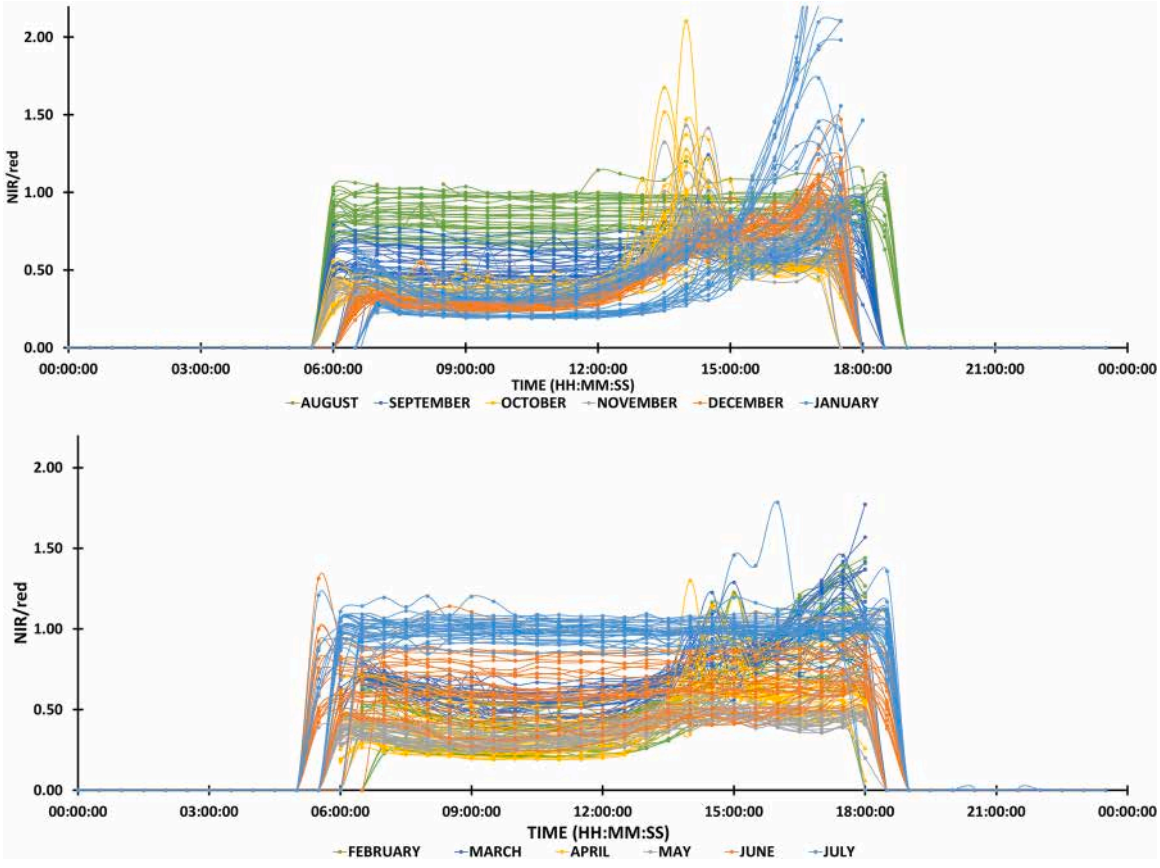

Fig. 6. Half hourly reflectance ratio (NIR/red index) for each day between the 1st of August 2018 and the 31th of July 2019. Night time data are set to zero.

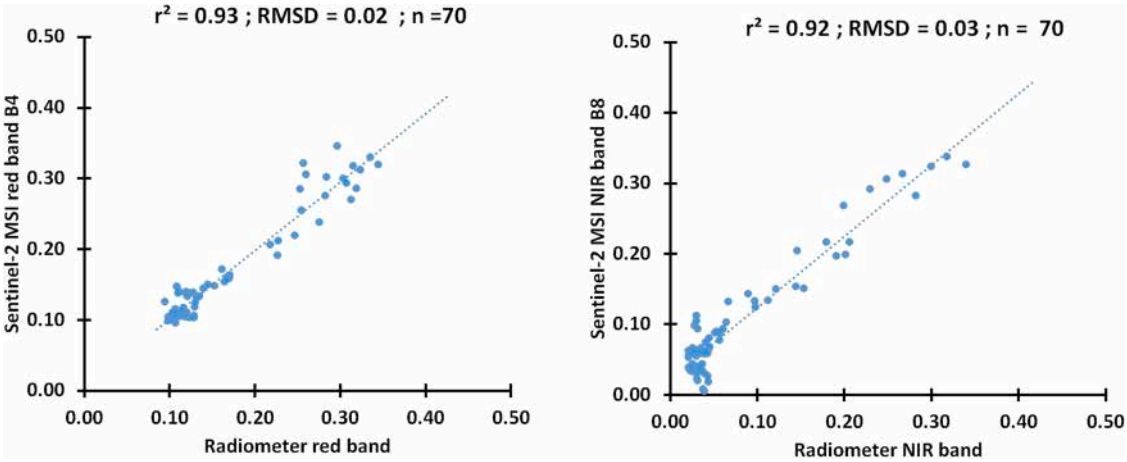

Fig. 7. Sentinel-2 MSI data vs SKYE reflectance in the red (left panel) and NIR (right panel) bands.

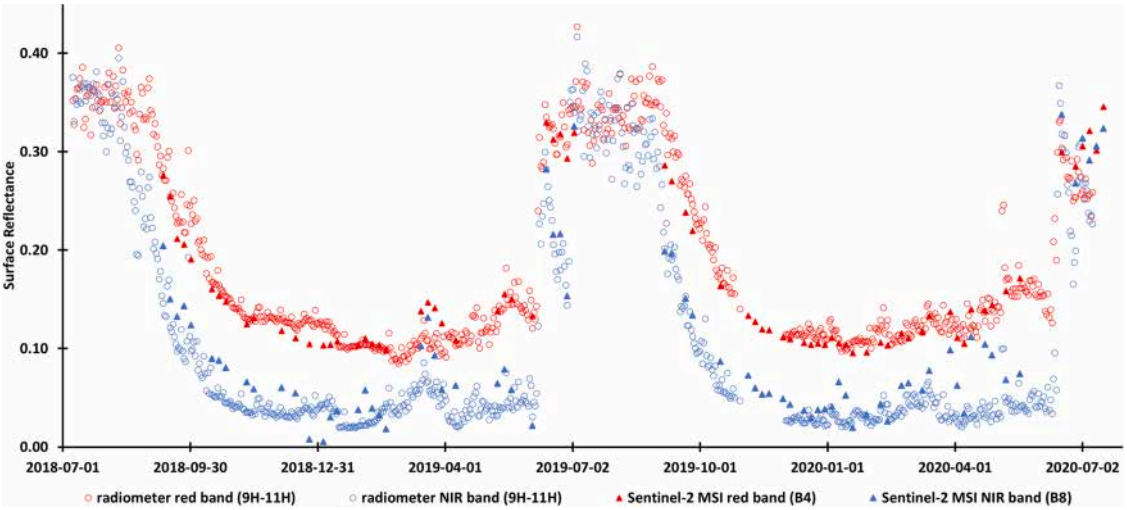

Fig. 8. Temporal evolution of the Niger water reflectance by the Sentinel-2 MSI and SKYE sensor in the red and near infrared bands.

$$[SPM] = 32{\cdot}7892 * (B8)^{2{\cdot}91417} \text{ (Sentinel-2 MSI)} \quad (3)$$

$$[SPM] = 1{\cdot}154 * (NIR/red)^{3{\cdot}430} \text{ (SKYE)} \quad (4)$$

where [SPM] is Suspended Particulate Matter concentration, B8 is the Sentinel-2 MSI Near infrared band, and NIR/red is the SKYE radiometer band ratio.

The retrieved SPM obtained by the two equations above are well correlated to in-situ SPM measurements with RMSE equal to 0.19 g L^{-1} and bias equal to 0.01 g L^{-1} for Sentinel-2 MSI and RMSE equal to 0.17 g L^{-1} and bias equal to 0.007 g L^{-1} for the radiometer. The r^2 quantifying the goodness of the fit between SPM measured and retrieved are equal to 0.84 for Sentinel-2 MSI and 0.90 for the in situ radiometer (Fig. 9c).

3.3. SPM dynamics and Niger River discharge

The evolution of SPM concentration is in phase advance in comparison to the river discharge dynamic (Fig. 10). At the beginning of the red flood period (June to September), the SPM concentration begins to increase and reaches its maximum at least one month before water level rises (Fig. 10) which is typically an effect of the first flush (Bertrand-Krajewski et al., 1998). The highest SPM concentrations of 0.5–2 g L^{-1} are measured during low (less than 500 m^3 s^{-1}) to medium (500–1000 m^3 s^{-1}) river discharge Then, while water discharge increases, the SPM concentration starts decreasing and continues to decrease during the peak of the red flood and afterwards (Fig. 11). When the black flood reached Niamey, the SPM concentration has already undergone a 10 time-decrease. This period is

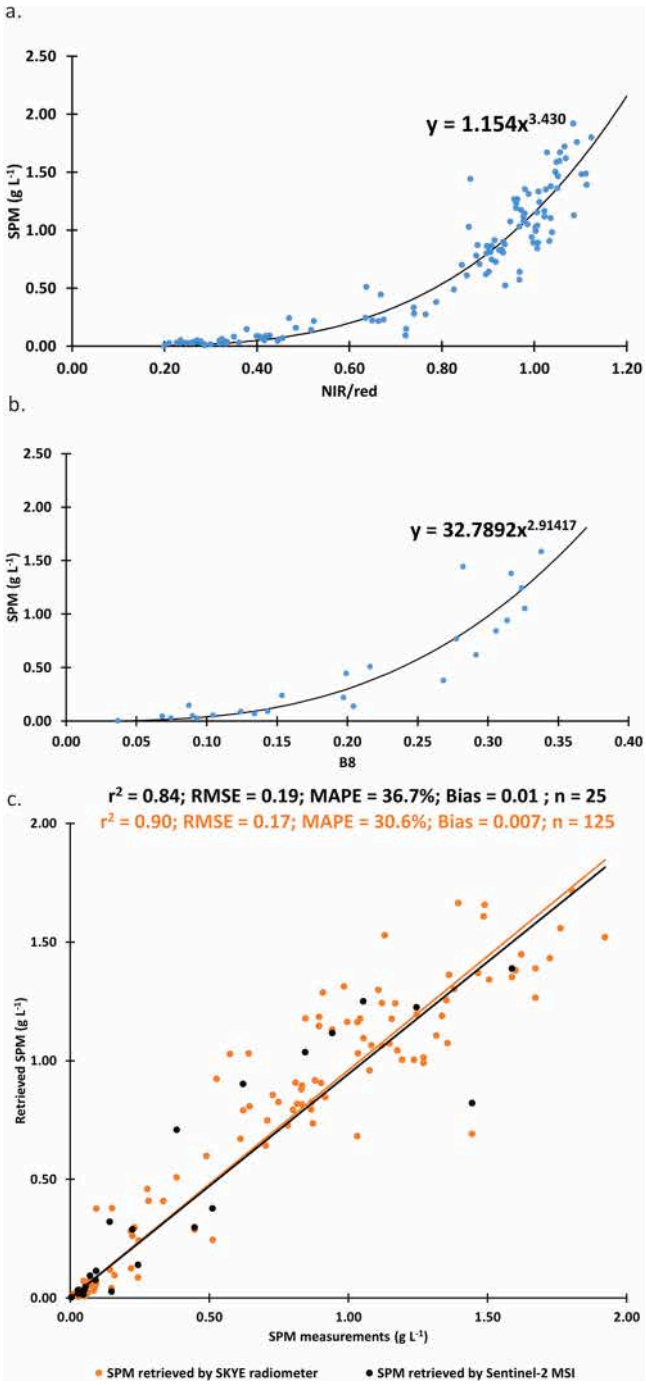

Fig. 9. top: Relationships between SKYE (a) and Sentinel-2 MSI (b) reflectances and in-situ SPM; bottom: Relationship between SPM retrieved by radiometric measurements and in-situ SPM (c). Note that the same samples are used in the top and bottom panels.

characterized by discharges that can approach 2000 $m^3 s^{-1}$ and low SPM concentration of about 0.1 g L^{-1}, i.e. 5 to more than 20 times lower than those measured during the red flood conditions (Fig. 11). When the black flood decreases the SPM concentration is still low, but shows some variations between February and April. The low water period displays the lowest discharge and SPM values around 0.01 g L^{-1}.

SPM interannual variability appears to be quite different at the beginning of the red flood with much lower SPM values in 2019 than in 2018 and 2020 during the month of June (Fig. 12). Interestingly, SPM values of those three years become more similar at the core of the red flood although a huge difference is observed in discharge. The highest discharge peak ever observed since the installation of the

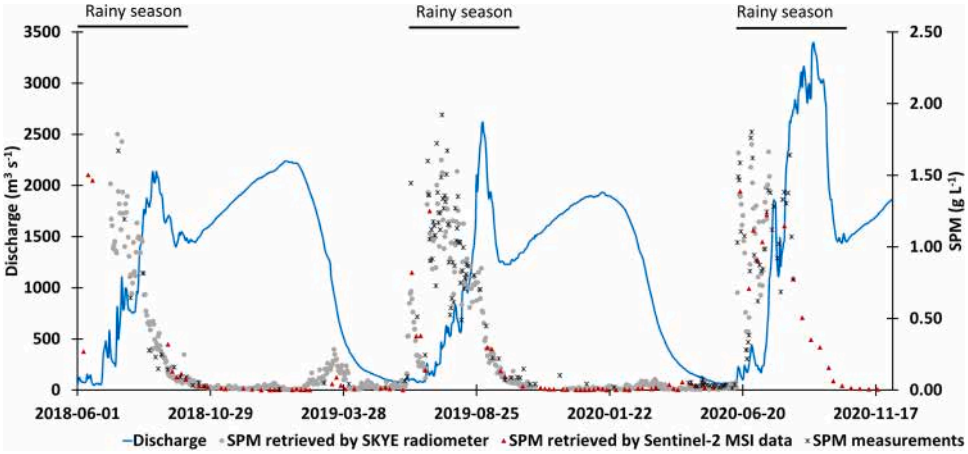

Fig. 10. Dynamics of SPM concentration and discharge at Niamey station between 2018 and 2020.

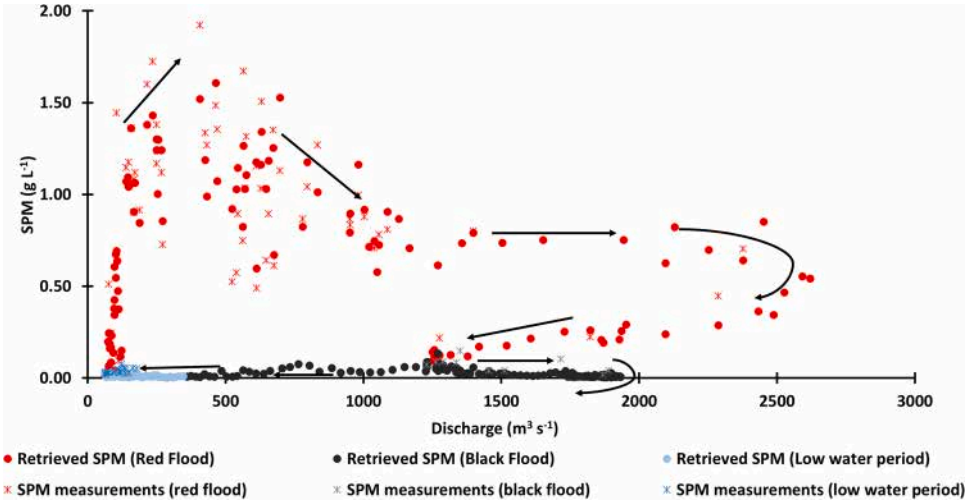

Fig. 11. SPM concentration (in-situ measurements and SKYE retrieval) vs discharge during the 2019 hydrological cycle at Niamey. The arrows represent the chronological evolution of the SPM concentration.

hydrographic station in the Niger River at Niamey occurred at the beginning of September 2020 (3398 $m^3 s^{-1}$). Despite this impressive discharge, the SPM concentration did not further increase and its value at this period in 2020 is similar with those observed in 2018 and slightly lower than the SPM values in 2019.

3.4. SPM spatial distribution and middle Niger basin contribution

The main tributaries of the Niger River contributing to the red flood are located downstream of Ansongo and the hydrographs at this location do not show the red flood discharge peak (Cassé et al., 2016). SPM concentrations retrieved from Sentinel-2 MSI are similar at Ansongo and Niamey during the black flood period, from October to May. During the rainy season (June – September periods), SPM peaks are observed at both locations, although with very different absolute values. While at Niamey the maximum concentration is about 1.5 g L^{-1}, at Ansongo it reaches only 0.15 g L^{-1} (Fig. 13). This clearly shows the role of the tributaries of the Middle Niger in the SPM routing to Niamey during the red flood. The average SPM difference between Niamey and Ansongo is equal to 0.185 g L^{-1} over this three-year period, 10 times higher than the mean SPM value at Ansongo for the same period.

The significant SPM contribution at the very beginning of the rainy season from the Sirba River (see the example in Fig. 14a, for the 17th of June 2020) further highlights this phenomenon. The Sirba river, a main tributary of the middle Niger River, contributes to 80% of the water supply recorded at the hydrological station of Niamey (Amani and Nguetora, 2002; Massazza et al., 2019). In contrast no major differences are found between the Sirba and the Niger river SPM concentration during the black flood (Fig. 14b).

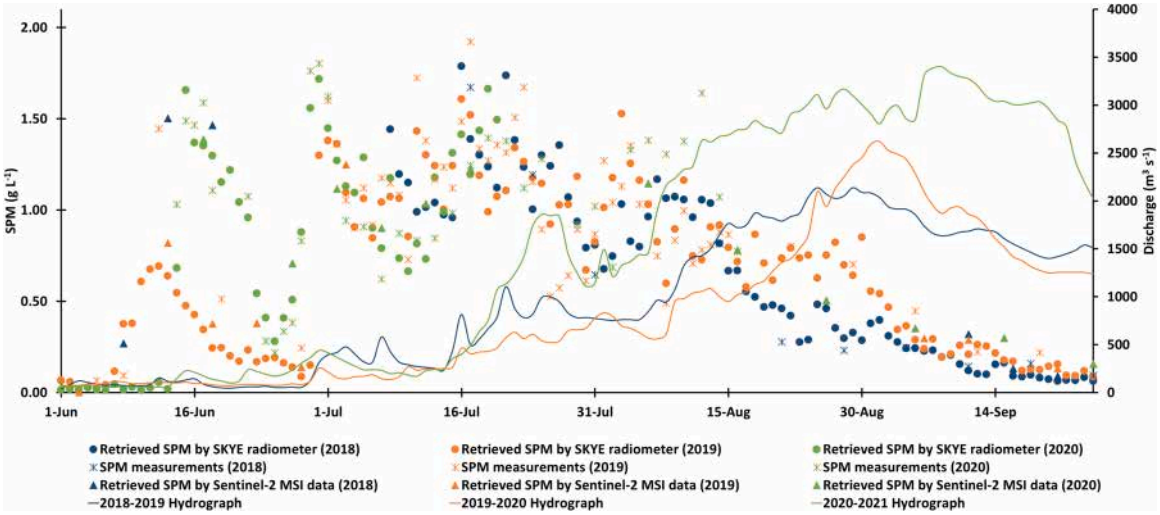

Fig. 12. Suspended particulate matter concentration retrieved and river discharge during the red flood in 2018, 2019 and 2020.

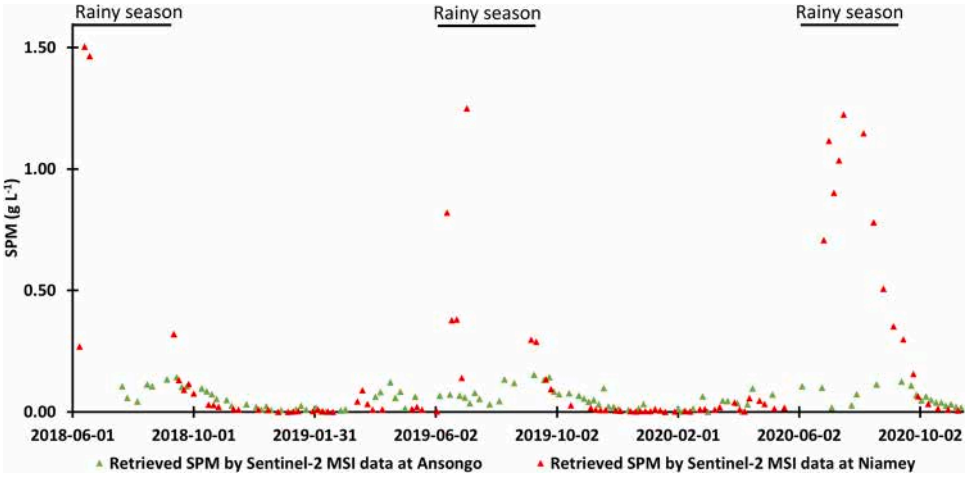

Fig. 13. Time series of Sentinel-2 MSI derived SPM at Niamey and Ansongo between 2018 and 2020.

4. Discussion

The aim of this study was to estimate the SPM spatio-temporal variability in MNRB combining available information by in-situ measurements and satellite data. Simple relationships were therefore used to retrieve SPM ad hoc for the study site from the SKYE and MSI reflectances, based on commonly employed power functions as in Robert et al. (2017). Reflectance measurements by in-situ and satellite measurements proved efficient to monitor the SPM dynamics in the middle Niger basin. The retrieval performances obtained by both SKYE and Sentinel-2 MSI are very good and generally better than those obtained by other optical remote sensing sensors such as MODIS and Landsat in the same region (Kaba et al., 2014; Robert et al., 2016; Robert et al., 2017). However, employing a multi-band approach according to the SPM range, as suggested by Novoa et al. (2017) and Han et al. (2016), may provide a good option to improve SPM retrievals and derive a robust relationship widely applicable over different water bodies.

Sunglint was found to significantly affect the in-situ radiometric measurements and reflectance as well as the band ratio. As a result, only a portion of the measurements acquired within a day can be used to investigate SPM dynamics at a sub-daily scale. This could be overcome by using several radiometers pointing at different directions or by applying sunglint correction based on the SWIR reflectance (Harmel et al., 2018). Skyglint was not corrected for and causes fluctuations in the NIR and red reflectance, especially for overcast mornings. The reflectance ratio is less affected by this effect. This may be the reason why the ratio is more efficient for SPM retrieval for all-sky radiometer data, as opposed to the NIR reflectance for Sentinel-2 MSI, for which clear-sky conditions are selected. Although it is not obvious on our data, heavy dust loadings may also impact the SKYE radiometer NIR and red reflectances, but probably less so the reflectance ratio.

Overall, the reflectance ratio data display relatively small variability during the morning period suggesting that varying cloudiness

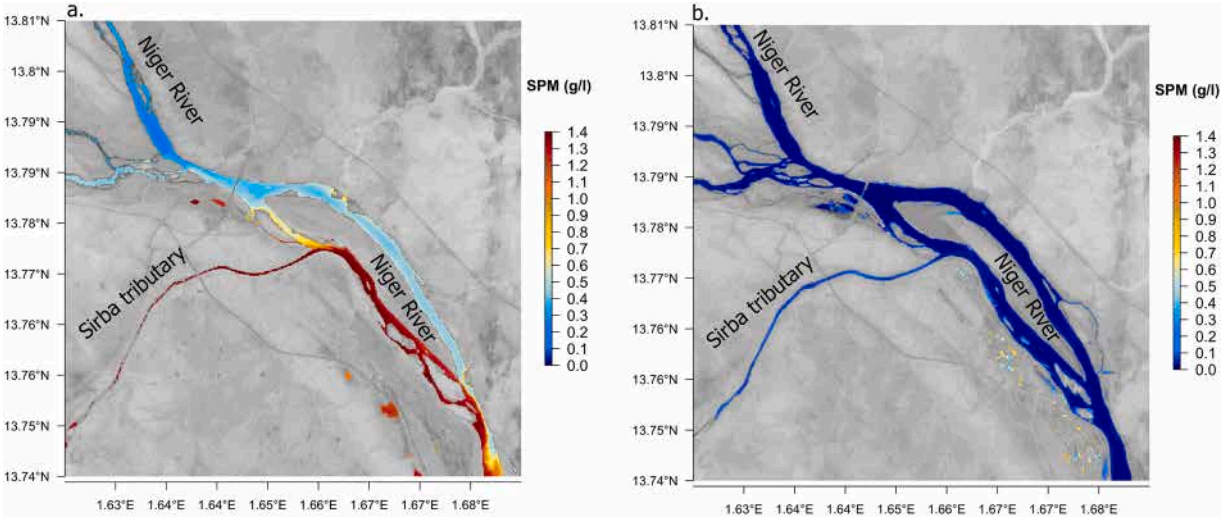

Fig. 14. Suspended particulate matter retrieved by Sentinel-2 MSI data showing input from the Sirba tributary.

or wind conditions are not major issues here and that rapid variability of SPM (sub-daily) is not common. The high values of the red and NIR reflectance in this river may attenuate sunglint and skyglint effects. Above-surface routine monitoring of water colour is mostly applied to ocean or coastal water where these issues are more severe (Mobley, 1999; Zibordi et al., 2009). The results shown in this study suggest that this kind of measurements could be used for tropical turbid rivers, either alone or in combination with high resolution satellite data.

Sentinel-2 MSI reflectance acquired for the Niamey station did not seem to be affected by sunglint problems: the Niamey station is located on the western edge of the Sentinel-2 swath and, given that the satellite overpasses at about 10h30 in the morning, specular reflection from the sun is unlikely at this site. This is not the case for the Ansongo site that is at the eastern edge of the Sentinel-2 swath and which may therefore be subject to sunglint effects. They would result in an overestimation of retrieved SPM at this site which would further increase the difference observed between Niamey and Ansongo and would not change our findings significantly.

Overall, the atmospheric correction scheme applied by the MAJA chain has proved accurate enough to monitor SPM variability. However, some issues remain. These concern particularly the impact of aerosols (mineral dust) on Sentinel-2 MSI reflectance, as indicated by the higher reflectance observed for Sentinel-2 MSI in both the NIR and the red band compared to SKYE reflectances in the March-April period (Fig. 8).

The SPM characteristics and their small size combined with their high concentration resulted in the very high values of reflectance observed in this area in both the visible and the NIR bands.

The nature of SPM in the Middle Niger at the latitude of Niamey is dominated by kaolinite, iron oxyhydroxides, and quartz. This composition is consistent with the nature of the sandy and sandy-silty Sahelian soils (Stroosnijder, 1982) and the outcropping rocks dominated by ferruginous sandstones of the terminal continental (Yaou et al., 2019). The iron oxyhydroxides would then come from the erosion of these surfaces. The kaolinite originates from the soils of the Middle Basin, which are recognized as not very reactive because of that kaolinitic nature (Mahamane et al., 2020).

SPM concentration showed an important intra-annual variability. The maximum concentration (~2 g L^{-1}) was recorded at the beginning of the rainy season (June - July). It was much higher than in the upper basins (0.6 g L^{-1} at Banankoro, Picouet et al., 2009) and lower than that observed on the Gorouol tributary at Alcongui (3.751 g L^{-1} in 2007/08, Amogu, 2009). The high SPM concentration in the middle part of the Niger River is likely related to the low vegetation cover at the beginning of the rainy season leading to strong soil erosion. Indeed, the soils have experienced significant crusting and increased erosion, resulting in tons of sediment drained into the river (Mamadou, 2012). Previous measurements of SPM concentration in the Middle Niger, although discontinuous, have shown quantities of the same order about 0.182 g L^{-1} to 1.5787 g L^{-1} (Alhou et al., 2016). In the major rivers of West Africa, the Senegal (Faye et al., 2020) and the Black Volta in Tanguasie (Bowan and Tingan, 2020), the concentrations of SPM measured were respectively 1.4 and 2.15 times lower than those of the Middle Niger River.

SPM concentration decrease observed during the rising water should rather be related to the conjugation of vegetation development on the water basin and the net decrease of the free elements in surfaces already washed out by the first rains. A similar decrease in SPM concentration occurring at the same period was observed in the Bangou Kirey Lake (located East of the Niamey) and ascribed to water dilution due to the rise in the water table (Abdourhamane Touré et al., 2016).

At the end of the black flood, close to the low water season, the SPM concentration displays a slight increase, in the absence of any input of water flow by runoff. This increase may be ascribed to the decrease in water volume leading to a local production of particles by the phenomenon of bank erosion. Alternatively, the March-April period is characterized by an increase in the speed of the trade winds (harmattan) that could stir the water and resuspend particles (Abdourhamane Touré et al., 2018). A similar increase in the middle of the dry season has been observed for Sahelian lakes in northern Mali (Robert et al., 2017), with wind-driven turbulence

possibly inducing a recirculation of bottom and bank sediments.

The SPM/Discharge hysteresis of the Niger River at Niamey are quite different from most hydrological systems. During the red flood the SPM/discharge curve follow the classic scenario observed in the Tropics with the maximum of SPM occurring before the discharge peak. This is the case for example at the Congo River outlet (N'kaya et al., 2020), for the Mississippi (Snedden et al., 2007) or Orinoco (Gallay et al., 2019). However, a major difference lies in the fact that the discharge curve of the Niger River at Niamey presents a second peak absent in these other systems. This peak is characterized by low SPM values which produce a distinctive feature for the middle Niger river. In terms of inter-annual variability, it is striking that the 2020 red flood, which was severe in Niamey, did not notably increase the river's SPM concentration.

5. Conclusion

This study has documented the SPM spatio-temporal variability in the middle Niger River.

Radiometric measurements collected in-situ or by satellite proved useful to monitor SPM which, in this area, is characterized by very fine kaolinite and iron oxyhydroxide particles that at high concentrations resulted in extremely high values of reflectance.

Good relationships were established between the radiometric measurements (NIR/red for SKYE in situ radiometer and NIR (B8) for Sentinel-2 MSI) and SPM concentration. This allowed to retrieve SPM concentration at Niamey at a daily time step (SKYE measurements) and to analyse their spatial variability within the middle Niger River (Sentinel-2 MSI). The red flood was characterised by very high SPM values with the SPM maximum reached at least one month before the maximum of the discharge, while low SPM values were recorded during the black flood. We have highlighted the important SPM contribution from the main tributary of the middle Niger River during the red flood which explains the difference in SPM between Niamey and Ansongo, located upstream. Finally, the interannual variability of SPM during the red flood was not found to play a major role on SPM concentration. In particular, SPM values after July in 2020 were similar to those in the previous two years, despite that record discharge values measured in 2020. However, future changes in SPM concentration under climate and anthropic changes, as for example the intensification of the hydrological cycle or the dam construction planned at the upstream on Niamey, and their impacts on SPM concentration in Niamey cannot be excluded and strongly underline the need to maintain monitoring of SPM in this area.

Author statement

Conceptualization, M.B.M., M.Gr., A.A.T., L.K., and E.R.; project administration, M.Gr.; investigation, M.B.M., M.Gr., A.A.T., L.K., B.L.; data acquisition, M.B.M., B.L., E.R-N., M.Go., B.A.T.; data analyzes, M.B.M., M.Gr., L.K., B.L.; writing-original draft preparation, M.B.M.; writing-review and edition, A.A.T., M.Gr., B.L., L.K., E.R., E.R-N.

Declaration of Competing Interest

The authors declare that they have no known competing financial interests or personal relationships that could have appeared to influence the work reported in this paper.

Acknowledgements

The authors would like to thank Adrien Paris for help with radiometer set up in Niamey, Franck Timouk for the radiometer configuration, Aliko Mamane for in-situ measurements and radiometer maintenance, Amelie Picot for the first granulometric measurements and data analysis and Guillaume Favreau for discussion on Niger River hydrology. We also thank Olivier Hagolle for discussions about the MAJA processing and anonymous reviewers for useful suggestions. The authors also acknowledge the "SEEN" (Société d'Exploitation des Eaux du Niger) for hosting the radiometer, IRD (Institut de Recherche pour le Développement) in Niamey for logistic help and the Goudel water treatment station manager and agents for allowing access to the sampling station. This study was supported by the French Centre National d'Etudes Spatiales (CNES) through the TELESSAO project (APR TOSCA Santé), by CREPE-NAAN project (INSU EC2CO) and by AMMA-CATCH observatory. This work is part of the Ph.D. thesis requirements on the first author (MBM) and was funded by "Institut de recherche pour le développement" (IRD) through ARTS program and the French Embassy in Niger through the "Service de coopération et d'action Culturelle (SCAC)".

References

Abdourhamane Touré, A., Guillon, R., Garba, Z., Rajot, J.L., Petit, C., Bichet, V., Durand, A., Sebag, D., 2010. Evolution des paysages sahéliens au cours des six dernières decennies dans la région de Niamey: de la disparition de la brousse tigrée à l'encroutement de surface des sols. Pangea /48), 47, pp. 35–40.

Abdourhamane Touré, A., Tidjani, A., Guillon, R., Rajot, J., Petit, C., Garba, Z., Sebag, D., 2016. Teneur en matières en suspension des lacs sahéliens en liaison avec les variations piézométrique et pluviométrique: cas des lacs Bangou Kirey et Bangou Bi, Sud-Ouest Niger. Afrique. Science 12 (2), 384–392.

Abdourhamane Touré, A., Tidjani, A.D., Rajot, J.L., Bouet, C., Garba, Z., Marticorena, B., Ambouta, K.J.M., 2018. Quantification des flux d'érosion éolienne au cours d'une transition champ-jachère au Sahel (Banizoumbou, Niger). Physio-Géo 12, 125–142. https://doi.org/10.4000/physio-geo.6287.

Alhou, B., Boukari, I., Darchambeau, F., 2016. Apports En Carbone Et Azote Dans Le Fleuve Niger À Tondibia (Niamey): Résultats De Deux (2) Ans D'observations. Eur. Sci. J. https://doi.org/10.19044/esj.2016.v12n21p167.

Allies, A., Demarty, J., Olioso, A., Bouzou Moussa, I., Issoufou, H.B.A., Velluet, C., Bahir, M., Maïnassara, I., Oï, M., Chazarin, J.P., Cappelaere, B., 2020. Evapotranspiration estimation in the Sahel using a new ensemble-contextual method. Remote Sens. 12 (3), 380. https://doi.org/10.3390/rs12030380.

Amani, A. and Nguetora, M., 2002. Evidence d'une modification du régime hydrologique du fleuve Niger à Niamey. IAHS PUBLICATION, pp.449–456.

Amogu, O., 2009. La dégradation des espaces sahéliens et ses conséquences sur l'alluvionnement du fleuve Niger moyen (Doctoral dissertation, University of Grenoble 1).

Amogu, O., Descroix, L., Yéro, K.S., Le Breton, E., Mamadou, I., Ali, A., Vischel, T., Bader, J.C., Moussa, I.B., Gautier, E., Boubkraoui, S., 2010. Increasing river flows in the Sahel ? Water 2 (2), 170–199. https://doi.org/10.3390/w2020170.

Autorité du Bassin du Fleuve Niger (ABFN), 2018. Rapport sur l'état du fleuve Niger au Mali. Avalaible on: https://q-eau-mali.net/media/rapport-sur-letat-du-fleuve-niger-au-mali/#:~:text=Le%20rapport%20permet%20de%20conna%C3%AEtre,et%20de%20plans%20d'actions (last Access: 17/01/2022).

Bertrand-Krajewski, J.L., Chebbo, G., Saget, A., 1998. Distribution of pollutant mass vs volume in stormwater discharges and the first flush phenomenon. Water Res. 32 (8), 2341–2356. https://doi.org/10.1016/S0043-1354(97)00420-X.

Billon, B., 1985. Le Niger à Niamey. Décrue et étiage 1985. Cah. Orstom. Série Hydrol. 21 (4), 3–22.

Bilotta, G.S., Burnside, N.G., Cheek, L., Dunbar, M.J., Grove, M.K., Harrison, C., Joyce, C., Peacock, C., Davy-Bowker, J., 2012. Developing environment-specific water quality guidelines for suspended particulate matter. Water Res. 46 (7), 2324–2332. https://doi.org/10.1016/j.watres.2012.01.055.

Bowan, P.A., Tingan, E.M.A., 2020. Influence of Illegal Small-Scale Gold Mining on the Black Volta Water. Commun. Appl. Sci. 9, 1–18.

Caballero, I., Steinmetz, F., Navarro, G., 2018. Evaluation of the first year of operational Sentinel-2A data for retrieval of suspended solids in medium-to high-turbidity waters. Remote Sens. 10 (7), 982. https://doi.org/10.3390/rs10070982.

Cassé, C., Gosset, M., Vischel, T., Quantin, G., Tanimoun, B.A., 2016. Model-based study of the role of rainfall and land use–land cover in the changes in the occurrence and intensity of Niger red floods in Niamey between 1953 and 2012. Hydrol. Earth Syst. Sci. 20 (7), 2841–2859. https://doi.org/10.5194/hess-20-2841-2016.

Dardel, C., Kergoat, L., Hiernaux, P., Grippa, M., Mougin, E., Ciais, P., Nguyen, C.C., 2014a. Rain-use-efficiency: What it tells us about the conflicting Sahel greening and Sahelian paradox. Remote Sens. 6 (4), 3446–3474. https://doi.org/10.3390/rs6043446.

Dardel, C., Kergoat, L., Hiernaux, P., Mougin, E., Grippa, M., Tucker, C.J., 2014b. Re-greening Sahel: 30 years of remote sensing data and field observations (Mali, Niger). Remote Sens. Environ. 140, 350–364. https://doi.org/10.1016/j.rse.2013.09.011.

Descroix, L., Genthon, P., Amogu, O., Rajot, J.L., Sighomnou, D., Vauclin, M., 2012. Change in Sahelian Rivers hydrograph: The case of recent red floods of the Niger River in the Niamey region. Glob. Planet. Change 98, 18–30. https://doi.org/10.1016/j.gloplacha.2012.07.009.

Descroix, L., Guichard, F., Grippa, M., Lambert, L.A., Panthou, G., Mahé, G., Gal, L., Dardel, C., Quantin, G., Kergoat, L., Bouaita, Y., 2018. Evolution of surface hydrology in the Sahelo-Sudanian strip: an updated review. Water 10 (6), 748. https://doi.org/10.3390/w10060748.

Descroix, L., Niang, A.D., Panthou, G., Bodian, A., Sane, Y., Dacosta, H., Abdou, M.M., Vandervaere, J.P., Quantin, G., 2015. Evolution récente de la pluviomètrie en Afrique de l'Ouest à travers deux régions: La sénégambie et le bassin du Niger moyen. Climatologie 12, 25–43. https://doi.org/10.4267/climatologie.1105.

Dieye M., Dia D., Barbier B., Sylla E.H.M., Sall M., Bader Jean-Claude, Bossa A.Y., Sanfo S., Fall C.S. (2020). L'agriculture de décrue en Afrique de l'Ouest et du centre: une certaine résilience face à la variabilité climatique et à la régulation des fleuves. In: Sultan Benjamin (ed.), Bossa A.Y. (ed.), Salack S. (ed.), Sanon M. (ed.). Risques climatiques et agriculture en Afrique de l'Ouest. Marseille: IRD, p. 121–131.

Doxaran, D., Froidefond, J.M., Lavender, S., Castaing, P., 2002. Spectral signature of highly turbid waters: application with SPOT data to quantify suspended particulate matter concentrations. Remote Sens. Environ. 81, 149–161.

Droy, I., Morand, P., 2013. Les grands aménagements sur le fleuve Niger: atout pour le Mali ou facteur de vulnérabilité pour ses populations rurales ? Mondes En. Dév. 164, 57–70. https://doi.org/10.3917/med.164.0057.

Drusch, M., Del Bello, U., Carlier, S., Colin, O., Fernandez, V., Gascon, F., Hoersch, B., Isola, C., Laberinti, P., Martimort, P., Meygret, A., 2012. Sentinel-2: ESA's optical high-resolution mission for GMES operational services. Remote Sens. Environ. 120, 25–36. https://doi.org/10.1016/j.rse.2011.11.026.

Favreau, G., Cappelaere, B., Massuel, S., Leblanc, M., Boucher, M., Boulain, N., Leduc, C., 2009. Land clearing, climate variability, and water resources increase in semiarid southwest Niger: a review. Water Resour. Res. 45 (7) https://doi.org/10.1029/2007WR006785.

Faye, C., Grippa, M., Kergoat, L., Robert, E., 2020. Investigating the drivers of total suspended sediment regime in the senegal river basin using landsat 8 satellite images. J. Environ. Geogr. 13 (1–2), 31–42 https://doi:10.2478/jengeo-2020-0004.

Gal, L., Grippa, M., Hiernaux, P., Pons, L., Kergoat, L., 2017. The paradoxical evolution of runoff in the pastoral Sahel: analysis of the hydrological changes over the Agoufou watershed (Mali) using the KINEROS-2 model. Hydrol. Earth Syst. Sci. 21 (9), 4591–4613. https://doi.org/10.5194/hess-21-4591-2017.

Gallaire, R., 1995. Données sur les transports du Niger moyen entre Kandadji et Niamey, in Grands Bassins Fluviaux Périatlantiques: Congo, Niger, Amazone, edited by J. C. Olivry and J. Boulègue, pp. 317–332, ORSTOM Editions, Paris.

Gallay, M., Martinez, J.M., Mora, A., Castellano, B., Yépez, S., Cochonneau, G., Alfonso, J.A., Carrera, J.M., López, J.L., Laraque, A., 2019. Assessing Orinoco river sediment discharge trend using MODIS satellite images. J. South Am. Earth Sci. 91, 320–331. https://doi.org/10.1016/j.jsames.2019.01.010.

Hagolle, O., Huc, M., Desjardins, C., Auer, S., and Richter, R., 2017. MAJA ATBD Algorithm Theoretical Basis Document, section 3.5 pg 31–37, CNES report 2017 (ref MAJA-TN-WP2–030 V1.0 2017/Dec/07) available on line at https://theia.sedoo.fr/wp-content-theia/uploads/sites/2/2018/12/atbd_maja_071217.pdf (last access: 04/05/2022).

Hagolle, O., Huc, M., Villa Pascual, D., Dedieu, G., 2015. A multi-temporal and multi-spectral method to estimate aerosol optical thickness over land, for the atmospheric correction of FormoSat-2, LandSat, VENμS and Sentinel-2 images. Remote Sens. 7 (3), 2668–2691. https://doi.org/10.3390/rs70302668.

Hamadou Younoussa, B., Hassane Yaou, T., Abdourhamane Touré, A., Moussa Issaka, A., Hassane, B., Garba, Z., 2020. Dynamique récente et actuelle de l'érosion en nappe aux abords du fleuve Niger. Afrique. Science 16 (1), 247–259.

Han, B., Loisel, H., Vantrepotte, V., Meriaux, X., Bryere, P., Ouillon, S., Dessailly, D., Xing, Q., Zhu, J., 2016. Development of a semi-analytical algorithm for the retrieval of suspended particulate matter from remote sensing over clear to very turbid waters. Remote Sens. 8. https://doi.org/10.3390/rs8030211.

Harmel, T., Chami, M., Tormos, T., Reynaud, N., Danis, P.A., 2018. Sunglint correction of the Multi-Spectral Instrument (MSI)-SENTINEL-2 imagery over inland and sea waters from SWIR bands. Remote Sens. Environ. 204, 308–321. https://doi.org/10.1016/j.rse.2017.10.022.

Hauer, C., Leitner, P., Unfer, G., Pulg, U., Habersack, H., Graf, W., 2018. The Role of Sediment and Sediment Dynamics in the Aquatic Environment. In: Schmutz, S., Sendzimir, J. (Eds.), Riverine Ecosystem Management, Aquatic Ecology Series, vol 8. Springer, Cham. https://doi.org/10.1007/978-3-319-73250-3_8.

Horiba. Partica LA950-V2. [En ligne]. Available on: http://www.horiba.com/fr/scientific/products/particle-characterization/particle-size-analysis/details/la-950-laser-particle-size-analyzer-108/ (last access: 11/01/2022).

2022 Anonhttps://worldpopulationreview.com/world-cities (last access: 11/01/2022).

2022 Anonhttps://www.skyeinstruments.com/ (last access: 11/01/2022).

Hulme, M., Doherty, R., Ngara, T., New, M., Lister, D., 2001. African climate change: 1900-2100. Clim. Res. 17 (2), 145–168.

Janicot, S., Moron, V., Fontaine, B., 1996. Sahel droughts and ENSO dynamics. Geophys. Res. Lett. 23 (5), 515–518. https://doi.org/10.1029/96GL00246.

Kaba, E., Philpot, W., Steenhuis, T., 2014. Evaluating suitability of MODIS-Terra images for reproducing historic sediment concentrations in water bodies: Lake Tana, Ethiopia. Int. J. Appl. Earth Obs. Geoinf. 26, 286–297. https://doi.org/10.1016/j.jag.2013.08.001.

Kuhn, C., de Matos Valerio, A., Ward, N., Loken, L., Sawakuchi, H.O., Kampel, M., Richey, J., Stadler, P., Crawford, J., Striegl, R., Vermote, E., 2019. Performance of Landsat-8 and Sentinel-2 surface reflectance products for river remote sensing retrievals of chlorophyll-a and turbidity. Remote Sens. Environ. 224, 104–118. https://doi.org/10.1016/j.rse.2019.01.023.

Lebel, T., Ali, A., 2009. Recent trends in the Central and Western Sahel rainfall regime (1990–2007). J. Hydrol. 375 (1–2), 52–64. https://doi.org/10.1016/j.jhydrol.2008.11.030.

Lebel, T., Panthou, G., Vischel, T., 2020. Inondations en Afrique: une nouvelle ère hydroclimatique. Conversat. Fr. 24.

Leblanc, M.J., Favreau, G., Massuel, S., Tweed, S.O., Loireau, M., Cappelaere, B., 2008. Land clearance and hydrological change in the Sahel: SW Niger. Glob. Planet. Change 61 (3–4), 135–150. https://doi.org/10.1016/j.gloplacha.2007.08.011.

Li, P., Ke, Y., Bai, J., Zhang, S., Chen, M., Zhou, D., 2019. Spatiotemporal dynamics of suspended particulate matter in the Yellow River Estuary, China during the past two decades based on time-series Landsat and Sentinel-2 data. Mar. Pollut. Bull. 149, 110518 https://doi.org/10.1016/j.marpolbul.2019.110518.

Liu, H., Li, Q., Shi, T., Hu, S., Wu, G., Zhou, Q., 2017. Application of sentinel 2 MSI images to retrieve suspended particulate matter concentrations in Poyang Lake. Remote Sens. 9 (7), 761. https://doi.org/10.3390/rs9070761.

Mahamadou, B.I., Bouzou Moussa, I., Faran Maiga, O., 2018. Évolution des caractéristiques pluviométriques et recrudescence des inondations dans les localités riveraines du fleuve Niger. VertigO-la Rev. électronique En. Sci. De. l'Environ. https://doi.org/10.4000/vertigo.19891.

Mahamane, M., Matchi, I.I., Hochschild, V., Mahamane, A., 2020. Évaluation du risque d'érosion du sol au Sahel: cas du paysage de Tillabéry. Afrique. SCIENCE 16 (5), 235–248.

Mahé, G., Lienou, G., Descroix, L., Bamba, F., Paturel, J.E., Laraque, A., Meddi, M., Habaieb, H., Adeaga, O., Dieulin, C., Chahnez Kotti, F., 2013. The rivers of Africa: witness of climate change and human impact on the environment. Hydrol. Process. 27 (15), 2105–2114. https://doi.org/10.1002/hyp.9813.

Mamadou, I., 2012. La dynamique accélérée des koris de la région de Niamey et ses conséquences sur l'ensablement du fleuve Niger (Doctoral dissertation, University of Grenoble 1 (France) and Université Abdou Moumouni de Niamey (Niger)), p.290.

Martinez, J.M., Guyot, J.L., Filizola, N., Sondag, F., 2009. Increase in suspended sediment discharge of the Amazon River assessed by monitoring network and satellite data. Catena 79 (3), 257–264. https://doi.org/10.1016/j.catena.2009.05.011.

Massazza, G., Tamagnone, P., Wilcox, C., Belcore, E., Pezzoli, A., Vischel, T., Panthou, G., Housseini Ibrahim, M., Tiepolo, M., Tarchiani, V., Rosso, M., 2019. Flood hazard scenarios of the Sirba River (Niger): evaluation of the hazard thresholds and flooding areas. Water 11 (5), 1018. https://doi.org/10.3390/w11051018.

Mobley, C.D., 1999. Estimation of the remote-sensing reflectance from above-surface measurements. Appl. Opt. 38 (36), 7442–7455.

N'kaya, G.D.M., Orange, D., Bayonne Padou, S.M., Datok, P., Laraque, A., 2020. Temporal variability of sediments, dissolved solids and dissolved organic matter fluxes in the Congo River at Brazzaville/Kinshasa. Geosciences 10 (9), 341. https://doi.org/10.3390/geosciences10090341.

Nechad, B., Ruddick, K.G., Park, Y., 2010. Calibration and validation of a generic multisensor algorithm for mapping of total suspended matter in turbid waters. Remote Sens. Environ. 114 (4), 854–866. https://doi.org/10.1016/j.rse.2009.11.022.

Nicholson, S.E., Tucker, C.J., Ba, M.B., 1998. Desertification, drought, and surface vegetation: an example from the West African Sahel. Bull. Am. Meteorol. Soc. 79 (5), 815–830. https://doi.org/10.1175/1520-0477(1998)079<0815:DDASVA>2.0.CO;2.

Niger Basin Nexus profile, 2018. Available on: https://www.water-energy-food.org/ru/resources/profil-nexus-bassin-du-niger (last access: 11/01/2022).

Novoa, S., Doxaran, D., Ody, A., Vanhellemont, Q., Lafon, V., Lubac, B., Gernez, P., 2017. Atmospheric Corrections and multi-conditional algorithm for multi-sensor remote sensing of suspended particulate matter in low-to-high turbidity levels coastal waters. Remote Sens. 9, 61. https://doi.org/10.3390/rs9010061.

Olivry, J.C., 2002. Synthèse des connaissances hydrologiques et potentiel en ressources en eau du fleuve Niger. Authority, Provisional Report. World Bank, Niger Basin, p. 160.

Pahlevan, N., Mangin, A., Balasubramanian, S.V., Smith, B., Alikas, K., Arai, K., Barbosa, C., Bélanger, S., Binding, C., Bresciani, M., Giardino, C., 2021. ACIX-Aqua: A global assessment of atmospheric correction methods for Landsat-8 and Sentinel-2 over lakes, rivers, and coastal waters. Remote Sens. Environ. 258, 112366 https://doi.org/10.1016/j.rse.2021.112366.

Pahlevan, N., Sarkar, S., Franz, B.A., Balasubramanian, S.V., He, J., 2017. Sentinel-2 MultiSpectral Instrument (MSI) data processing for aquatic science applications: demonstrations and validations. Remote Sens. Environ. 201, 47–56. https://doi.org/10.1016/j.rse.2017.08.033.

Panthou, G., Lebel, T., Vischel, T., Quantin, G., Sane, Y., Ba, A., Ndiaye, O., Diongue-Niang, A., Diopkane, M., 2018. Rainfall intensification in tropical semi-arid regions: The Sahelian case. Environ. Res. Lett. 13 (6), 064013 https://doi.org/10.1088/1748-9326/aac334.

Paturel, J.E., Poussin, J.C., Braquet, N., Ferry, L., Mahé, G., Ogilvie, A., Diello, P., Hertzog, T., 2020. Avenir du Fleuve Niger. 204. ⟨https://www.documentation.ird.fr/hor/fdi:010080259⟩.

Pennock, J.R., Sharp, J.H., 1994. Temporal alternation between light-and nutrientlimitation of phytoplankton production in a coastal plain estuary. Mar. Ecol. Prog. Ser. 275–288.

Petus, C., Chust, G., Gohin, F., Doxaran, D., Froidefond, J.M., Sagarminaga, Y., 2010. Estimating turbidity and total suspended matter in the Adour River plume (South Bay of Biscay) using MODIS 250-m imagery. Cont. Shelf Res. 30 (5), 379–392. https://doi.org/10.1016/j.csr.2009.12.007.

Picouet, C., Hingray, B., Olivry, J.C., 2009. Modelling the suspended sediment dynamics of a large tropical river: the Upper Niger River basin at Banankoro. Hydrol. Process.: Int. J. 23 (22), 3193–3200. https://doi.org/10.1002/hyp.7398.

Pinet, S., Martinez, J.M., Ouillon, S., Lartiges, B., Villar, R.E., 2017. Variability of apparent and inherent optical properties of sediment-laden waters in large river basins–lessons from in situ measurements and bio-optical modeling. Opt. Express 25 (8), A283–A310. https://doi.org/10.1364/OE.25.00A283.

Renosh, P.R., Doxaran, D., Keukelaere, L.D., Gossn, I.J., 2020. Evaluation of atmospheric correction algorithms for sentinel-2-MSI and sentinel-3-OLCI in highly turbid estuarine waters. Remote Sens. 12 (8), 1285. https://doi.org/10.3390/rs12081285.

Robert, E., Grippa, M., Kergoat, L., Pinet, S., Gal, L., Cochonneau, G., Martinez, J.M., 2016. Monitoring water turbidity and surface suspended sediment concentration of the Bagre Reservoir (Burkina Faso) using MODIS and field reflectance data. Int. J. Appl. Earth Obs. Geoinf. 52, 243–251. https://doi.org/10.1016/j.jag.2016.06.016.

Robert, E., Grippa, M., Nikiema, D.E., Kergoat, L., Koudougou, H., Auda, Y. and Rochelle-Newall, E., 2021. Environmental determinants of E. coli, link with the diarrheal diseases, and indication of vulnerability criteria in tropical area (Kapore, Burkina Faso). medRxiv. https://doi.org/10.1101/2021.04.21.21255867.

Robert, E., Kergoat, L., Soumaguel, N., Merlet, S., Martinez, J.M., Diawara, M., Grippa, M., 2017. Analysis of suspended particulate matter and its drivers in Sahelian ponds and lakes by remote sensing (Landsat and MODIS): Gourma region, Mali. Remote Sens. 9 (12), 1272. https://doi.org/10.3390/rs9121272.

Rochelle-Newall, E., Nguyen, T.M.H., Le, T.P.Q., Sengtaheuanghoung, O., Ribolzi, O., 2015. A short review of fecal indicator bacteria in tropical aquatic ecosystems: knowledge gaps and future directions. Front. Microbiol. 6, 308. https://doi.org/10.3389/fmicb.2015.00308.

Shen, F., Verhoef, W., Zhou, Y., Salama, M.S., Liu, X., 2010. Satellite estimates of wide-range suspended sediment concentrations in Changjiang (Yangtze) estuary using MERIS data. Estuar. Coast 33, 1420–1429.

Snedden, G.A., Cable, J.E., Swarzenski, C., Swenson, E., 2007. Sediment discharge into a subsiding Louisiana deltaic estuary through a Mississippi River diversion. Estuar. Coast. Shelf Sci. 71 (1–2), 181–193. https://doi.org/10.1016/j.ecss.2006.06.035.

Stroosnijder, L., 1982. La pédologie du Sahel et du terrain d'étude. In La productivite des paturages Saheliens. In Penning de Vries M.A. Djiteye F.W.T No., 918, 1982, pp. 52–71.

Taylor, C.M., Belušić, D., Guichard, F., Parker, D.J., Vischel, T., Bock, O., Harris, P.P., Janicot, S., Klein, C., Panthou, G., 2017. Frequency of extreme Sahelian storms tripled since 1982 in satellite observations. Nature 544 (7651), 475–478. https://doi.org/10.1038/nature22069.

Tidjani, A.D., 2008. Erosion éolienne dans le Damagaram Est (Sud-Est du Niger): paramétrisation, quantification et moyens de lutte. (Doctoral dissertation, Univ. Catholique de Louvain), p.171.

Tiepolo, M., Belcore, E., Braccio, S., Issa, S., Massazza, G., Rosso, M., Tarchiani, V., 2021. Method for fluvial and pluvial flood risk assessment in rural settlements. MethodsX 8, 101463. https://doi.org/10.1016/j.mex.2021.101463.

World Bank 2017. Republic of Niger, Priorities for ending poverty and boosting shared prosperity: systematic country diagnostic. Report No. 115661-NE, pp126. Available at: https://openknowledge.worldbank.org/handle/10986/28994?show=full&locale-attribute=fr.

Yaou, T.H., Younoussa, B.H., Abdourhamane Touré, A., Issaka, A.M., Hassane, B., Garba, Z., 2019. Analyse géomorphologique des risques liés aux mouvements de terrain à Niamey. Niger. Rev. Ivoir. Sci. Technol. 34, 247–263.

Zheng, G., DiGiacomo, P.M., 2017. Uncertainties and applications of satellite-derived coastal water quality products. Prog. Oceanogr. 159, 45–72. https://doi.org/10.1016/j.pocean.2017.08.007.

Zibordi, G., Berthon, J.F., Mélin, F., D'Alimonte, D., Kaitala, S., 2009. Validation of satellite ocean color primary products at optically complex coastal sites: Northern Adriatic Sea, Northern Baltic Proper and Gulf of Finland. Remote Sens. Environ. 113 (12), 2574–2591. https://doi.org/10.1016/j.rse.2009.07.013.